Journal of Hazardous Materials 209–210 (2012) 264–270

Contents lists available at SciVerse ScienceDirect

Journal of Hazardous Materials

journal homepage: www.elsevier.com/locate/jhazmat

Effect of natural organic matter on the aggregation kinetics of CeO_2 nanoparticles in KCl and $CaCl_2$ solutions: Measurements and modeling

Kungang Li, Yongsheng Chen*

School of Civil and Environmental Engineering, Georgia Institute of Technology, Atlanta, GA 30332, United States

ARTICLE INFO

Article history:
Received 26 October 2011
Received in revised form
18 December 2011
Accepted 4 January 2012
Available online 12 January 2012

Keywords:
Nanoparticle
Aggregation
Natural organic matter
DLVO
EDLVO

ABSTRACT

To characterize the environmental transport and quantify the risk of nanoparticles (NPs), it is important to fundamentally understand the aggregation of NPs and to describe this process quantitatively. This study investigates the aggregation kinetics of CeO_2 NPs in the presence of KCl, $CaCl_2$ and humic acid (HA) using time-resolved dynamic light scattering. In KCl solutions, regardless of their concentration, HA drastically reduces the aggregation kinetics of CeO_2 NPs. However, the effect of HA was more complicated in $CaCl_2$ solutions. At low $CaCl_2$ concentrations, HA inhibited NP aggregation, whereas at high $CaCl_2$ concentrations, HA promoted aggregation. The critical coagulation concentration (CCC) in KCl in the absence of HA is approximately 36.5 mM. In presence of both 1 ppm and 10 ppm HA in KCl solutions, extremely low aggregation kinetics were observed even at very high KCl concentrations (500 mM), implying KCl–CCCs in presence of HA were larger than 500 mM. The CCCs under conditions of no HA, 1 ppm HA and 10 ppm HA in $CaCl_2$ solutions are approximately 9.5, 8.0 and 12.0 mM, respectively. These observations were analyzed in the framework of extended Derjaguin–Landau–Verwey–Overbeek (EDLVO) theory. Moreover, a kinetic model was used to predict the aggregation kinetics of CeO_2 NPs. The model predictions are in close agreement with experimental observations. To the best of our knowledge, this work is the first to model quantitatively the aggregation of NPs in the presence of natural organic matter.

© 2012 Elsevier B.V. All rights reserved.

1. Introduction

The nanoscience and nanotechnology boom of recent years has demonstrated that nanotechnology will play a significant role in advancing the technologies of the 21st century in many sectors (e.g., pharmaceutical, energy, electronic and textile) [1]. Engineered nanoparticles (NPs) probably will be released into the aquatic environment through manufacturing processes, waste disposal or product uses; however, insufficient research has examined the environmental behavior of NPs [2]. There are only limited data available on aggregation and deposition of NPs. Especially, theoretical analysis and quantitative models are insufficiently developed to quantify the environmental transport and fate of NPs [3].

Given the unique properties of NPs, they could constitute a new class of nonbiodegradable pollutants that aquatic organisms may uptake and food webs may transfer, and thus they could affect ecosystems and human health. It is imperative to evaluate the risks of NPs to avoid repeating past environmental tragedies. The groundwork for the risk assessment of NPs is the characterization of their physicochemical states (e.g., size, shape, surface charge), which greatly influence their stability, mobility, bioavailability and toxicity [4]. However, ambient factors [e.g., pH, ionic strength, presence of natural organic matter (NOM)] could change the state of NPs and result in a dynamic system. A pivotal process that leads to dynamic changes in the states of NPs is aggregation, which alters their size and shape. A number of studies have reported that the size of nanoparticles was an important factor in determining their toxicity [5–8]. Aggregation will change the size of nanoparticles and thus very likely change their toxicity. Investigation of NP aggregation is thus important for evaluating their environmental fate and assessing their risk, and aggregation studies of NPs are gaining popularity [3].

Aggregation data can be obtained through either case-by-case experiments or theoretical approaches. Because many solution or medium chemistries exist and the number of engineered NPs is expected to increase rapidly in the near future [9], case-by-case studies would be time consuming and expensive. The theoretical approach is more appropriate to assess the aggregation of NPs in the environment. Fundamentally, the interfacial forces/energies between interacting particles control aggregation. In aquatic environments, solution chemistries strongly influence the interfacial forces/energies between NPs and therefore greatly determine their aggregation. For example, several studies showed that increasing ionic strength tends to promote the aggregation of NPs [10–12], because it weakens their repulsive electrostatic (EL) force. The conventional Derjaguin–Landau–Verwey–Overbeek (DLVO) theory

* Corresponding author. Tel.: +1 404 894 3089.
E-mail address: yongsheng.chen@ce.gatech.edu (Y. Chen).

0304-3894/$ – see front matter © 2012 Elsevier B.V. All rights reserved.
doi:10.1016/j.jhazmat.2012.01.013

was developed by balancing the attractive van der Waals (vdW) force and EL force [13,14], and it interprets the impact of ionic strength on particle aggregation.

However, much evidence indicates that even in a simple system with only salt and NPs present, classical DLVO theory is limited when attempting to describe particle aggregation quantitatively; a sizable discrepancy still exists between theoretical predictions and experimental observations [15]. This is because non-DLVO forces may also play important roles between particles [16]. For example, in aqueous media, the polar Lewis acid/base (AB) force [17], which is the sum of the hydrogen-bonding force, hydrophobic interaction force and hydration force [16–18], may account for approximately 90% of all non-covalent forces [17]. Moreover, NOM such as humic acid (HA) and fulvic acids is ubiquitous in natural environments, and a more realistic investigation of NP aggregation may need to involve the NOM in the system. In solutions containing monovalent electrolytes (e.g., KCl and NaCl), HA probably increases the stability of NPs regardless of the ionic strength [11]. However, aggregation becomes remarkably complicated in the presence of Ca^{2+} [11,12], which is the predominant ion in groundwater and river water samples [19]. For example, HA stabilized C_{60} NPs at low $CaCl_2$ concentrations, whereas it enhanced C_{60} aggregation at high $CaCl_2$ concentrations [11]. NOM is expected to adsorb onto the NP surface, which alters the physicochemical properties of NPs and thus the interfacial forces/energies between them. It has been suggested that NOM might introduce a steric force [16] and a bridging force [20,21] as well as perturb vdW attraction, EL repulsion and AB interaction [21]. Consequently, non-DLVO forces must be incorporated in a precise theoretical analysis of NP interaction and a quantitative description of the aggregation process. This analysis is known as the extended DLVO theory (EDLVO or XDLVO) approach [17], which provides a more solid theoretical basis. However, to the best of our knowledge, few published studies employ the EDLVO approach to model the aggregation of NPs theoretically.

CeO_2 NP was used as a model NP in this study because it has extensive commercial applications [4,22,23] and thus is very likely to be released into the environment. The Organization for Economic CO-operation and Development (OECD) has listed CeO_2 NPs as one of priority nanomaterials for immediate testing [24]. We investigated the effect of Suwannee River HA on the aggregation of CeO_2 NPs in KCl and $CaCl_2$ using time-resolved dynamic light scattering (TR-DLS). The aggregation tendency or attachment efficiency was derived from experimental results. Moreover, a kinetic model combining EDLVO theory and von Smoluchowski's population balance equation was used to predict the aggregation kinetics of CeO_2 NPs, which were then compared with experimental data. To the best of our knowledge, this study is the first to model quantitatively the aggregation kinetics of NPs in the presence of NOM.

2. Materials and methods

2.1. Materials

CeO_2 NP suspension with a nominal size of 25 nm was purchased from Sigma–Aldrich. The atomic compositions of the sample were verified by X-ray diffraction technique (data not shown). The pH of the stock suspension was 4.5 as measured by pH meter (Accumet model 15, Fisher Scientific). The concentration of the stock suspension was 109.5 g/L, and for the aggregation experiments, 10 mg/L dilutions were made with 18 MΩ deionized (DI) water unless otherwise indicated. KCl and $CaCl_2$ stock solutions were prepared using ACS reagent-grade chemicals and were filtered through 0.02-μm filters before use. The Suwannee River Humic Acid (SRHA or HA) (standard II, 2S101H, International Humic Substances Society) solution was prepared by dissolving 100 mg SRHA standard II in 250 mL DI water; the solution was then filtered through 0.4-μm membrane filters that were pre-dried at 60 °C in an oven overnight. The membrane filters were dried under the same conditions after use. The final HA concentration was determined by the filter weight difference. The HA solution was stored in the dark at 4 °C. Primary properties of SRHA, such as the molecular weight (range of 1–5 kDa) and composition, have been reported elsewhere [25].

2.2. Characterization of CeO_2 NPs

The morphology of CeO_2 NPs was determined by transmission electron microscopy (TEM). Samples were prepared by depositing 5 μL of CeO_2 NP suspension on a copper grid (400-mesh size) coated with carbon film (Ted Pella, Redding, CA). A Philips EM420 model TEM was operated at an accelerating voltage of 210 kV to acquire images. Particle size distribution (PSD) was obtained using DLS on a Zetasizer Nano ZS instrument (Malvern Instruments). In brief, 1.5 mL of CeO_2 NP suspension was injected into a clean cuvette, and the DLS instrument was then operated with a scattering angle of 173° from the incident laser beam, and the autocorrelation function automatically accumulated at least 10 runs for each sample. The electrophoretic mobilities (EPMs) of CeO_2 NPs were measured for a range of K^+ and Ca^{2+} concentrations in the presence and absence of HA using the Zetasizer Nano ZS instrument. At least four parallel measurements were made for each condition. To minimize the interference of aggregation, measurements began immediately after the desired conditions were achieved.

2.3. Aggregation kinetics

The aggregation kinetics experiments were carried out at pH 5.7, at which the CeO_2 NPs are stable for at least 24 h (see Fig. S1 in the SI). The pH values of the CeO_2 NP, KCl, $CaCl_2$ and HA solutions were pre-adjusted to 5.7 to ensure that each measurement could start immediately after addition of K^+, Ca^{2+} and HA. For the aggregation experiments in the absence of HA, a premeasured amount of KCl or $CaCl_2$ was added to 1 mL of CeO_2 NP suspension in a cuvette. The NP suspension was then shaken slightly and placed in the Zetasizer. For the experiment in the presence of HA, a premeasured amount of HA stock solution was added to the NP suspension along with the KCl or $CaCl_2$. The effect of HA concentration was investigated with two concentrations, 1 ppm and 10 ppm.

2.4. Modeling the aggregation kinetics

The adsorption of HA alters the physicochemical properties of the CeO_2 NP surface by introducing steric and bridging forces as well as by perturbing vdW attraction, EL repulsion and AB interaction [21]. The vdW attraction is affected because HA adsorption alters the particle size and the Hamaker constant [26]. The HA layer also alters the surface charge density, or surface potential, of NPs, which further affects the EL repulsion [27]. In addition, HA adsorption alters the surface electron-acceptor or electron-donor properties, which changes the AB interaction [17]. The total interaction energy (V_T) between HA-coated particles is computed by assuming that each force acts individually and is thus additive: $V_T = V_{vdW} + V_{EL} + V_{HA} + V_{AB}$. Detailed computation methods for each interaction energy are presented in S1 in the supporting information (SI).

Upon computing the total interaction energy (V_T), the aggregation kinetics of CeO_2 NPs can be obtained on the basis of Eq. (1) [28]:

$$r = a \cdot \left\{ 1 + \frac{4k_B T n_0}{3\mu W} t \right\}^{1/d_F} \quad (1)$$

where a is the primary particle radius, k_B is the Boltzmann constant, T is the absolute temperature, μ is the viscosity of the solution (8.90×10^{-4} Pa s), n_0 is the initial number concentration of primary particles, d_F is the fractal dimension of aggregates, and t is the time. W is the stability ratio, which can be expressed as [10,29]:

$$W = \left[\int_0^\infty \lambda(u)\frac{\exp(V_T(u)/kT)}{(2+u)^2}du\right] \cdot \left[\int_0^\infty \lambda(u)\frac{\exp(V_A(u)/kT)}{(2+u)^2}du\right]^{-1} \quad (2)$$

where u is the normalized surface-to-surface separation distance (h) between two particles ($u = h/a$). $V_A(u)$ is the attractive energy. vdW energy is the only contributing term to $V_A(u)$ for bare particles. However, for particles coated with HA, the bridging attraction contributes as well. $\lambda(u)$ is the correction factor for the diffusion coefficient, which is related to the separation distance by Eq. (3) [30]:

$$\lambda(u) = \frac{6(u)^2 + 13(u) + 2}{6(u)^2 + 4(u)} \quad (3)$$

Eq. (1) was derived to describe the diffusion-limited aggregation. In this study, we attempted to apply it in the initial radius-growth stage of reaction-limited aggregation as well. This is because the aggregate structure might not greatly influence the particle collision efficiency in the early stage of reaction-limited aggregation; moreover, a rigorous expression does not exist for describing the reaction-limited aggregation [28,31]. However, as aggregation proceeds, the aggregate structure indeed affects particle collision efficiency, which implies that Eq. (1) may be invalid in modeling reaction-limited aggregation beyond the early stage.

The number concentration of CeO_2 NPs is determined from the mass concentration. The lattice parameter (a_l) of CeO_2 unit cells is 5.4087 Å [32], and each unit cell contains four Ce atoms and eight O atoms. The number of Ce atoms (N) per CeO_2 NP with radius r can be calculated using Eq. (4).

$$N = 4 \times \frac{(4/3)\pi r^3}{a_l^3} = \frac{16}{3}\pi\left(\frac{r}{a_l}\right)^3 \quad (4)$$

The mass of a single CeO_2 NP is then obtained, and the number concentration of NPs can be computed.

3. Results and discussion

3.1. Characterization of CeO_2 NPs

A TEM image of CeO_2 NPs is presented in Fig. S2 in the SI. The NPs are close to spherical in shape and have a relatively uniform size distribution. The inset in Fig. S2 shows the PSD diagrams of CeO_2 NPs in the absence and presence of HA; these diagrams are obtained from DLS measurements. The NP size measured with DLS is greater than that determined with TEM, which is consistent with previous studies [33,34]. This is probably caused by some minor particle aggregation or the thickness of the adsorbed water layer on the NP surfaces. The average hydrodynamic radii of CeO_2 NPs in the absence of HA and in the presence of 1 ppm and 10 ppm HA are 50.7, 52.5, and 55.0 nm, respectively. The polydispersity indices (PDI) are quite small (~0.1), indicating that CeO_2 NPs are highly monodispersed. Fig. 1 shows the EPMs of CeO_2 NPs under different HA concentrations in KCl and $CaCl_2$ solutions. In the absence of HA, the CeO_2 NPs are positively charged at pH 5.7. However, with HA present, the surface charge (potential) of CeO_2 NPs shifts to the negative domain, which indicates HA adsorption onto the CeO_2 NPs. Because the HA was introduced into the NP suspension just before the EPM measurements, this verified that HA adsorption occurred almost immediately. The EPMs under all conditions

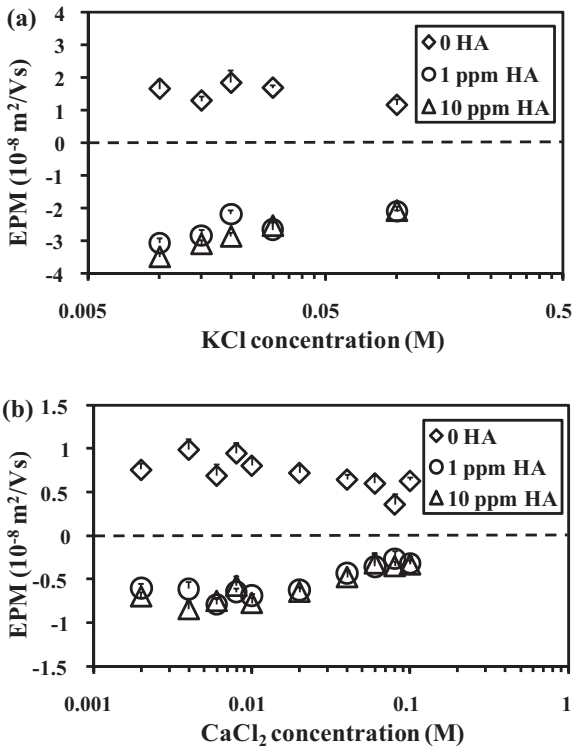

Fig. 1. Electrophoretic mobilities (EPMs) of CeO_2 NPs under different HA concentrations in (a) KCl and (b) $CaCl_2$.

tended to become less positive (no HA) or less negative (1 and 10 ppm HA) as ionic strength increased, which was caused by the compressed electrical double layer and by cation binding to the carboxylic functional groups of HA adsorbed on the NPs [11,35]. Although the magnitude of the EPMs is expected to decrease continuously with increasing ionic strength owing to compression of the electrical double layer and neutralization of surface charge, Fig. 1 reveals that the general shape of the mobility curves exhibits an extremum at moderate ionic strength. Similar trends have been reported elsewhere [36,37] and might be explained by the preferential adsorption of co-ions onto the NP surface, which results in a decrease in the electrokinetic potential [37,38]. Fig. 1 also reveals that the divalent ions (Ca^{2+}) are more effective in screening the NP surface charge than monovalent ions (K^+). The EPMs were further converted to zeta potential via the Henry equation (see SI) [39]. Although the presence of HA changed the sign of the particle surface charge, in $CaCl_2$ solution the absolute values of the EPMs/zeta potentials changed only slightly, which means that the EL repulsion force did not change greatly in the presence of HA. However, the impact of HA on CeO_2 NP stability was significant (see next section). This observation suggested that non-DLVO forces played an important role in the system.

3.2. Influence of HA on the aggregation of CeO_2 NPs in KCl and $CaCl_2$

Fig. S4 in the SI shows representative aggregation kinetics profiles of CeO_2 NPs in KCl and $CaCl_2$ solutions in the absence and presence of HA as obtained from TR-DLS measurements. The initial number concentration of CeO_2 NPs is approximately 2.35×10^{15} particles/m^3 in all aggregation experiments. HA stabilizes CeO_2 NPs at all KCl concentrations. In the presence of a relatively low concentration of HA (1 ppm), the CeO_2 NPs were stabilized, and no aggregation was observed even at a high KCl concentration (0.1 M) (Fig. S4a in the SI). When a higher HA

concentration was applied (10 ppm), the aggregation of CeO_2 NPs further decreased, and no aggregation was observed even when the KCl concentration increased to 0.5 M. This stabilizing effect of NOM also has been reported in other studies [11,40]. However, in $CaCl_2$ solutions, the behavior of the NPs was more complicated. At low Ca^{2+} concentration (0.004 M), the aggregation rate of CeO_2 NPs is inhibited in the presence of HA, possibly because of steric repulsion due to the adsorption of HA molecules onto NPs, which greatly stabilizes the system. However, at high $CaCl_2$ concentration (0.08 M), HA enhanced the aggregation of CeO_2 NPs, probably owing to the bridging attraction between CeO_2 NPs, which is induced by the HA aggregates formed through intermolecular bridging via Ca^{2+} complexation [11,41].

The attachment efficiencies (α), or inverse stability ratios ($1/W$), were calculated by normalizing the initial slopes of the aggregation curves with those obtained in the diffusion-limited aggregation regime (presented in Fig. S5). Since extremely low aggregation kinetics were observed even at high KCl concentrations in the presence of HA, the attachment efficiency profiles were not produced with KCl in the presence of HA. Two distinct aggregation regimes, diffusion limited and reaction limited, are observed in the absence of HA. The CCCs were determined by the intersection of two lines extrapolated through the reaction-limited and diffusion-limited regimes (not shown here owing to the crowding). In the absence of HA, the CCCs were approximately 36.5 mM in KCl and 9.5 mM in $CaCl_2$ solutions. In the presence of HA, diffusion-limited and reaction-limited regimes were also observed in $CaCl_2$ solution, which was consistent with other studies [42]. Moreover, in $CaCl_2$ solution, the attachment efficiency was smaller in the presence of HA than in its absence in the reaction-limited regime but larger in the diffusion-limited regime. However, the enhancement of the aggregation rate by HA in high concentrations of $CaCl_2$ was not as great as that in other NP systems, such as silicon and fullerene [11,42]. The CCCs under no HA, 1 ppm HA and 10 ppm HA conditions are approximately 9.5, 8.0 and 12.0 mM, respectively, which indicates that the HA concentration has an influence on the CCC.

3.3. Model parameter determination and interaction energy analysis

Because the aggregation process is fundamentally controlled by the interaction forces/energies between NPs, computing the interaction energy enables us to better understand the effect of HA on aggregation. Eqs. (S1)–(S4) in the SI were employed to compute each interaction energy term (V_{vdW}, V_{EL}, V_{HA} and V_{AB}) and the total interaction energy (V_T). Those equations involve many parameters that could be measured experimentally or computed theoretically. However, some measurements and calculations are extremely challenging, and thus, inevitably, some parameters must be estimated. For example, ΔG_{h0}^{AB} for bulk materials might be determined by contact angle measurements. However, for nanoscale materials, whose physiochemical properties greatly differ from their bulk counterparts, the contact angle measurement is not applicable. Although parameter estimation could have been achieved by "artificial" optimization, this can result in physically unrealistic values. In this study, most parameters were determined through experiments or obtained from the literature. In brief, the surface potentials (ψ_S) of CeO_2 NPs under different solution chemistries were calculated from the EPMs, as mentioned in SI. The adsorbed HA-layer thicknesses (δ) were measured by DLS rather than calculated from Ohshima's soft particle theory [43,44] because the primary NPs are highly monodispersed in the system. The δ values obtained in this study are consistent with those reported earlier [45]. Consistent with another study [21], a value of 0.5 was assigned to the fractional HA surface coverage (Γ/Γ_0) in the presence of 10 ppm HA; in the presence of 1 ppm HA, Γ/Γ_0values were determined from adsorption experiments. The Hamaker constant of bare CeO_2 NPs, the term $\alpha S_c k_B T/a_m^3$, the scaling length (D_{Sc}), and the HA volume fraction at the NP surface (Φ_{S0}) were obtained or estimated from the literature [21,46–49]. The calculation of the Hamaker constant of HA-coated NPs is presented in Section S8. The only remaining parameter, ΔG_{h0}^{AB}, was adjusted to make the theoretically calculated attachment efficiencies match the experimentally derived ones. The attachment efficiencies, or the inverse stability ratios ($1/W$), were then computed according to Eq. (2).

$V_T(u)$, the total interaction energy between NPs separated by a normalized distance u, can be computed as discussed above. $V_A(u)$ is the attractive energy. For bare particles, vdW energy is the only contributing term for $V_A(u)$. However, for particles coated with HA, the bridging attraction should be incorporated as well. For the primary parameters used in the computation of attachment efficiencies, refer to Table S1 in the SI.

The ΔG_{h0}^{AB} values fell into the narrow ranges of 2.0–2.6 mJ/m^2 for bare CeO_2 NPs in KCl, 2.7–3.0 mJ/m^2 for bare CeO_2 NPs in $CaCl_2$, and 0.15–0.7 mJ/m^2 for HA-coated CeO_2 NPs in $CaCl_2$, which have the same order of magnitude as the values for other metal oxides [50,51]. Although ΔG_{h0}^{AB} is expected to be constant in the same type of electrolyte, it exhibits narrow distributions. This might be caused by error in EPM measurements, i.e., the EPMs we obtained were not 100% accurate owing to the instrument deviations. Moreover, converting EPMs to zeta potentials and then to surface potentials using approximation equations introduces deviations. Errors in the size measurements and adsorption experiments, the approximation equations in the EDLVO analysis, and the numerical integration used in Matlab also lead to the ΔG_{h0}^{AB} value distributions. The ΔG_{h0}^{AB} value for the bare CeO_2 NPs used in this study is slightly larger than that for another type of bare CeO_2 NPs that are larger, as discussed in our previous study [28]; this is reasonable because the hydrophilicity of metal oxide NPs is size dependent, and larger size might lead to smaller hydrophilicity and thus a smaller ΔG_{h0}^{AB} value [52].

It is difficult to quantify the magnitude of each interaction energy term for cases in the presence of HA in KCl solution because almost no aggregation was observed under those conditions. Moreover, theoretical calculations showed that, regardless of the steric force, the increased EL force and decreased vdW force owing to the introduction of HA results in marked repulsion among CeO_2 NPs and then stabilizes the system. Consequently, V_{HA}, V_{AB}, and relevant parameters cannot be determined in the presence of HA in KCl solution.

On the basis of the parameters listed in Table S1, the interaction energy profiles for CeO_2 NPs under representative solution chemistries are computed and presented in Fig. 2. The energy barrier reflects the aggregation tendency. In the absence of HA in 0.1-M KCl solution, no energy barrier is observed, which indicates that the aggregation of CeO_2 NPs is within the diffusion-limited regime. However, a high barrier (approximately 50 kT) arose with the introduction of HA into the system, and correspondingly, the aggregation of NPs did not occur under those conditions. In 0.004-M $CaCl_2$, the magnitude of the energy barrier decreases in the order 10 ppm HA, 1 ppm HA, and no HA, which implies that the aggregation rate increases in the same order. The experimental data shown in Fig. S4b in the SI prove this. Moreover, in 0.08-M $CaCl_2$ solution, no energy barrier is observed under all conditions; however, Fig. S4c in the SI shows that the aggregation rate under 10 ppm HA is higher than that under the other two conditions. This indicates that the energy barrier cannot be used as a quantitative index. Therefore, a more complicated, but quantitative, index involving integration, as shown in Eq. (2), was used to compute the aggregation efficiency.

To better understand the contribution of each interaction energy term, the representative profiles were plotted and are presented in Fig. S7a. Steric repulsion clearly contributes greatly, whereas EL

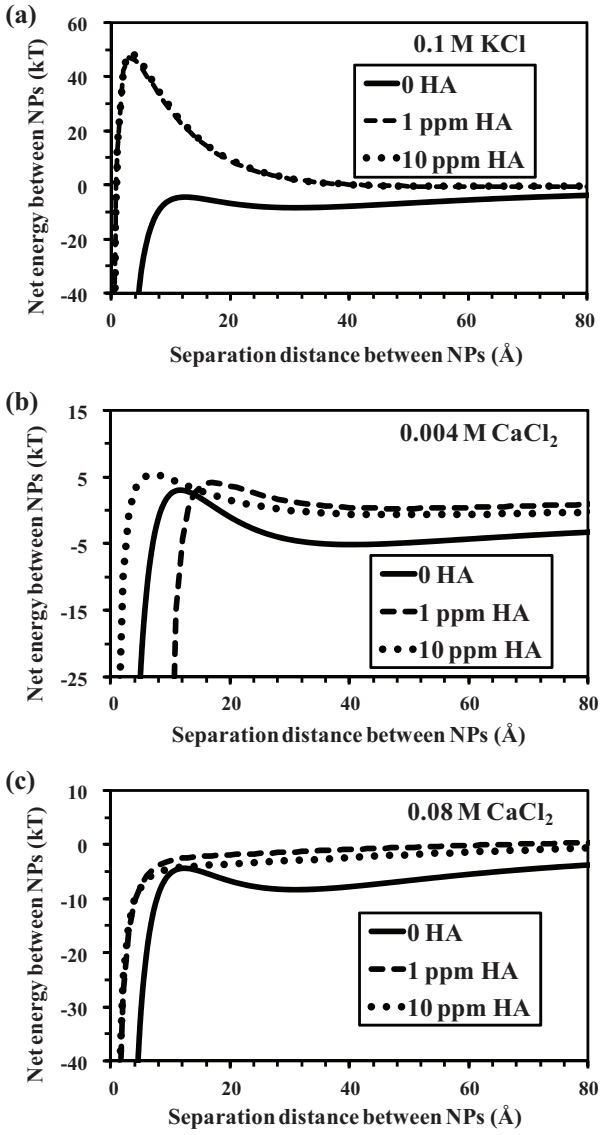

Fig. 2. Interaction energy profiles of CeO_2 NPs in the absence and presence of HA under (a) 0.1 M KCl, (b) 0.004 M $CaCl_2$ and (c) 0.08 M $CaCl_2$. The continuous, dashed and dotted lines are model simulations corresponding to 0, 1 ppm and 10 ppm HA, respectively.

repulsion does not, which implies that screening surface charges by counter-ions may not be crucial for the aggregation. Fig. S7b compares each energy term in the absence and presence of 10 ppm HA in 0.002 M $CaCl_2$ solution. The vdW attractive force decreased in the presence of HA, mainly because of the smaller Hamaker constant. EL repulsion remains almost constant because, although HA adsorption changed the sign of the NP surface charge, the absolute values are similar. In addition, owing to smaller ΔG_{h0}^{AB} value for HA-coated NPs, the AB force decreased with HA present in the solution. The total energy barrier increased in the presence of HA, which means that HA stabilized CeO_2 NPs in the solution. In some other cases, the energy barrier decreased in the presence of HA, and thus HA destabilized NPs.

3.4. Modeling the aggregation kinetics of CeO_2 NPs

Eq. (1) was used to model the aggregation kinetics of CeO_2 NPs. The fractal dimension d_F is widely acknowledged to be ~1.8 for diffusion-limited aggregation and ~2.1 for reaction-limited aggregation [53–56] (see Table S2 in the SI). V_T and n_0 were computed

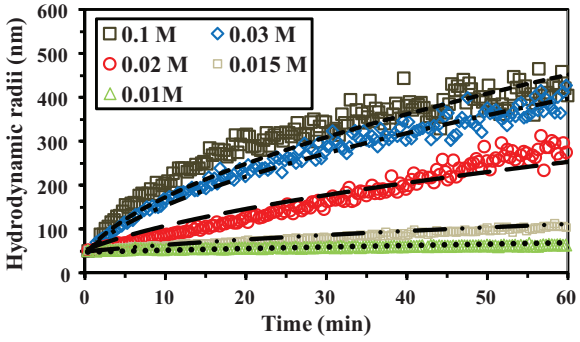

Fig. 3. Comparison of the simulated and experimental time evolution of the hydrodynamic radii of CeO_2 NPs in the absence of HA in KCl solutions. The lines are model simulations.

as discussed earlier, and other parameters are located in Table S1. Representative computed results are compared with experimental data in Figs. 3 and 4. Because including all aggregation data for $CaCl_2$ in Fig. 4 makes it too crowded, we present the rest of the data

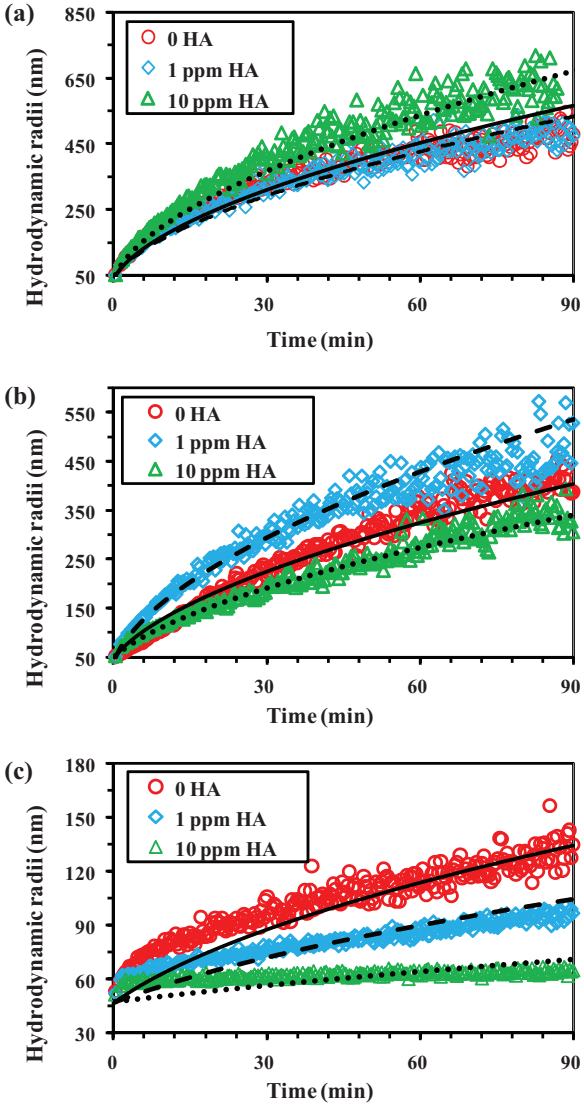

Fig. 4. Comparison of the simulated and experimental time evolution of the hydrodynamic radii of CeO_2 NPs under (a) 0.08 M, (b) 0.008 M and (c) 0.004 M $CaCl_2$ solutions. The continuous, dashed and dotted lines are model simulations corresponding to the conditions of 0, 1 ppm and 10 ppm HA, respectively.

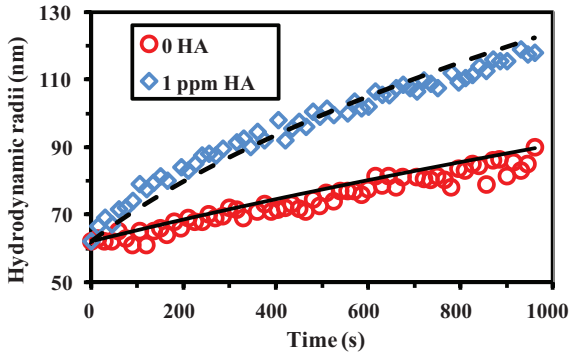

Fig. 5. Comparisons of the simulated and experimental time evolution of the hydrodynamic radii of fullerene NPs in the absence and presence of HA (1 mg/L total organic carbon (TOC)) under solution conditions of 40 mM $CaCl_2$. The continuous and dashed lines are model simulations corresponding to the conditions of 0 and 1 ppm HA, respectively. Good agreements were reached under those two conditions. The experimental data were obtained from Ref. [7].

in Fig. S8. Model predictions and experimental observations closely agreed under various solution chemistries. The model predictions could be further improved to match the experimental observations by optimizing the d_F values. However, we did not do that in order to avoid introducing any physically unrealistic values from the blind optimization. It is worth noted that Eq. (1) was derived for diffusion-limited aggregation. However, the close agreements shown in this study indicate that the equation also could be applicable to the initial aggregation stage (<1.5 h) in the reaction-limited aggregation regime. The discrepancies between model predictions and experimental data can be attributed to several causes. First, it is difficult to accurately determine the surface potential of NPs, particularly in the presence of HA. Second, the primary NPs were assumed to be uniform in size, which is reasonable given the small PDI, but a narrow particle size distribution does exist. Third, HA adsorption was assumed to occur uniformly on all NPs, whereas in reality, non-uniform adsorption and disproportionate surface coverage occurred. Finally, to simplify the computation, HA adsorption was assumed to reach equilibrium before the NPs aggregated, which is reasonable because the adsorption is fast and the preliminary experiments showed that a rough equilibrium is attained within minutes. However, the adsorption kinetics should be incorporated into a more accurate model.

3.5. Application of the aggregation kinetics model to other NP systems

The aggregation kinetics model was tested via application to other NP systems in the presence and absence of NOM. We compared our model computations with the experimental data of Chen et al. [11] and Saleh et al. [12,40]. In Chen et al. [11], the early stage aggregation kinetics of fullerene (C_{60}) NPs in the absence and presence of HA was investigated, and the attachment efficiencies and representative aggregation profiles were presented. Because the study did not provide EPMs and HA adsorption data, we cannot calculate the particle interaction energy (V_T) theoretically using Eq. (1). Instead, we obtained the value of the W in Eq. (1) from the attachment efficiency profile. The initial fullerene NP concentration, n_0, is 1.6×10^{14} particles/m^3. We calculated the aggregation kinetics according to Eq. (1) and compared it with the experimental data (presented in Fig. 5). The fractal dimension d_F was 1.8 and 2.2 for the conditions of no HA and 1 ppm HA, respectively; this is reasonable because in the presence of HA, the aggregates formed are in a loose structure and therefore have a higher d_F value. It is worth noted that although HA may interact with Fullerene and CeO_2 with π–π interactions and chemical bonding in the particle-HA intersurface, respectively, in our case the focus was the interaction between NPs coated with HA, which are analogous between Fullerene and CeO_2. HA molecules were found to adsorb onto both types of NPs, thus both NPs would become HA-coated particles and the interaction between two such particles were analogous.

Although the model was developed on the basis of the interaction of spherical particles, we tested it on both multiwalled carbon nanotubes (MWNTs) and single-walled carbon nanotubes (SWNTs). Comparisons between model calculations and experimental data are presented in Fig. S9 in the SI. A surprisingly good agreement was reached, which implies that our model is probably applicable to nanomaterials other than spherical NPs.

4. Conclusion

In summary, NP aggregation is governed by the interaction force/energy; through computation of this, we are able to determine the aggregation tendency and aggregation kinetics of NPs in different solutions. This work attempted to model the aggregation kinetics of CeO_2 NPs by integrating surface force theories in the presence of HA. The model predictions were compared with experimental data and agreed well. To the best of our knowledge, this is the first attempt to quantitatively model the NP aggregation process in the presence of NOM, and the reported results indicate that the model could be applied in both monovalent and divalent ionic solutions. All of the parameters in the model are physically meaningful and were obtained, as far as possible, from experimental studies rather than blind optimization or fitting. Moreover, the computation is relatively less demanding than computer simulations, and thus the model is suitable for pre-evaluation of the aggregation tendency of NPs under different conditions. This theoretical analysis and modeling lays the groundwork for prediction of the aggregation process of NPs in complex aquatic environments, which greatly influences their fate and biological effects as reported by a number of previous studies [3,5–8]. Therefore, this work could contribute to the risk assessment of NPs.

Acknowledgments

This study was partially supported by the US Environmental Protection Agency Science to Achieve Results Program Grant RD-83385601 and Engineering Research Center (ERC)/Semiconductor Research Corporation (SRC)/ESH Grant (425.025).

Appendix A. Supplementary data

Supplementary data associated with this article can be found, in the online version, at doi:10.1016/j.jhazmat.2012.01.013.

References

[1] T. Xia, N. Li, A.E. Nel, Potential health impact of nanoparticles, Annu. Rev. Publ. Health 30 (2009) 137–150.
[2] A. Helland, M. Scheringer, M. Siegrist, H.G. Kastenholz, A. Wiek, R.W. Scholz, Risk assessment of engineered nanomaterials: a survey of industrial approaches, Environ. Sci. Technol. 42 (2008) 640–646.
[3] A.R. Petosa, D.P. Jaisi, I.R. Quevedo, M. Elimelech, N. Tufenkji, Aggregation and deposition of engineered nanomaterials in aquatic environments: role of physicochemical interactions, Environ. Sci. Technol. 44 (2010) 6532–6549.
[4] S.J. Klaine, P.J.J. Alvarez, G.E. Batley, T.F. Fernandes, R.D. Handy, D.Y. Lyon, S. Mahendra, M.J. McLaughlin, J.R. Lead, Nanomaterials in the environment: Behavior, fate, bioavailability, and effects, Environ. Toxicol. Chem. 27 (2008) 1825–1851.
[5] B.D. Chithrani, W.C.W. Chan, Elucidating the mechanism of cellular uptake and removal of protein-coated gold nanoparticles of different sizes and shapes, Nano Lett. 7 (2007) 1542–1550.
[6] M. Lundqvist, J. Stigler, G. Elia, I. Lynch, T. Cedervall, K.A. Dawson, Nanoparticle size and surface properties determine the protein corona with possible implications for biological impacts, Proc. Natl. Acad. Sci. U.S.A. 105 (2008) 14265–14270.

[7] A.E. Nel, L. Madler, D. Velegol, T. Xia, E.M.V. Hoek, P. Somasundaran, F. Klaessig, V. Castranova, M. Thompson, Understanding biophysicochemical interactions at the nano-bio interface, Nat. Mater. 8 (2009) 543–557.
[8] A. Verma, F. Stellacci, Effect of surface properties on nanoparticle-cell interactions, Small 6 (2010) 12–21.
[9] T. Puzyn, B. Rasulev, A. Gajewicz, X.K. Hu, T.P. Dasari, A. Michalkova, H.M. Hwang, A. Toropov, D. Leszczynska, J. Leszczynski, Using nano-QSAR to predict the cytotoxicity of metal oxide nanoparticles, Nat. Nanotechnol. 6 (2011) 175–178.
[10] K.L. Chen, M. Elimelech, Aggregation and deposition kinetics of fullerene (C-60) nanoparticles, Langmuir 22 (2006) 10994–11001.
[11] K.L. Chen, M. Elimelech, Influence of humic acid on the aggregation kinetics of fullerene (C-60) nanoparticles in monovalent and divalent electrolyte solutions, J. Colloid Interface Sci. 309 (2007) 126–134.
[12] N.B. Saleh, L.D. Pfefferle, M. Elimelech, Aggregation kinetics of multiwalled carbon nanotubes in aquatic systems: measurements and environmental implications, Environ. Sci. Technol. 42 (2008) 7963–7969.
[13] L.D.L.B.V. Derjaguin, Theory of stability of highly charged lyophobic sols and adhesion of highly charged particles in solutions of electrolytes, Acta Physicochim. 14 (1941) 633.
[14] E.J.W. Verwey, J.T.G. Overbeek, K.v. Nes, Theory of the Stability of Lyophobic Colloids: The Interaction of Sol Particles Having an Electric Double Layer, Elsevier Pub. Co., New York, 1948.
[15] S.H. Behrens, D.I. Christl, R. Emmerzael, P. Schurtenberger, M. Borkovec, Charging and aggregation properties of carboxyl latex particles: experiments versus DLVO theory, Langmuir 16 (2000) 2566–2575.
[16] D. Grasso, K. Subramaniam, M. Butkus, K. Strevett, J. Bergendahl, A review of non-DLVO interactions in environmental colloidal systems, Rev. Environ. Sci. Biotechnol. 1 (2002) 17–38.
[17] C.J. Van Oss, Interfacial Forces in Aqueous Media, 2nd ed., Taylor & Francis, Boca Raton, FL, 2006.
[18] J. Israelachvili, H. Wennerstrom, Role of hydration and water structure in biological and colloidal interactions, Nature 379 (1996) 219–225.
[19] A.A. Keller, H.T. Wang, D.X. Zhou, H.S. Lenihan, G. Cherr, B.J. Cardinale, R. Miller, Z.X. Ji, Stability and aggregation of metal oxide nanoparticles in natural aqueous matrices, Environ. Sci. Technol. 44 (2010) 1962–1967.
[20] T.L. Byrd, J.Y. Walz, Interaction force profiles between Cryptosporidium parvum oocysts and silica surfaces, Environ. Sci. Technol. 39 (2005) 9574–9582.
[21] V. Runkana, P. Somasundaran, P.C. Kapur, A population balance model for flocculation of colloidal suspensions by polymer bridging, Chem. Eng. Sci. 61 (2006) 182–191.
[22] G. Aguila, F. Gracia, P. Araya, CuO and CeO_2 catalysts supported on Al_2O_3, ZrO_2, and SiO_2 in the oxidation of CO at low temperature, Appl. Catal. A: Gen. 343 (2008) 16–24.
[23] K. Kaneko, K. Inoke, B. Freitag, A.B. Hungria, P.A. Midgley, T.W. Hansen, J. Zhang, S. Ohara, T. Adschiri, Structural and morphological characterization of cerium oxide nanocrystals prepared by hydrothermal synthesis, Nano Lett. 7 (2007) 421–425.
[24] Organization for Economic Co-operation and Development. List of manufactured nanomaterials and list of endpoints for phase one of the sponsorship programme for the testing of manufactured nanomaterials: revision. Series on the Safety of Manufactured Nanomaterials No. 27, 2010. http://www.oecd.org/officialdocuments/displaydocumentpdf?cote=env/jm/mono%282010%2946&doclanguage=en (accessed on 10.08.11).
[25] S.K. Hong, M. Elimelech, Chemical and physical aspects of natural organic matter (NOM) fouling of nanofiltration membranes, J. Membr. Sci. 132 (1997) 159–181.
[26] J. Israelachvili, Intermolecular and Surface Forces, 2nd ed., Academic Press, London; San Diego, 1991.
[27] H. Ohshima, Theory of Colloid and Interfacial Electric Phenomena, Academic Press, Amsterdam; London, 2006.
[28] K.G. Li, W. Zhang, Y. Huang, Y.S. Chen, Aggregation kinetics of CeO_2 nanoparticles in KCl and $CaCl_2$ solutions: measurements and modeling, J. Nanopart. Res., in press.
[29] D.N.L. Mcgown, G.D. Parfitt, Improved theoretical calculation of stability ratio for colloidal systems, J. Phys. Chem. 71 (1967) 449–450.
[30] E.P. Honig, G.J. Roeberse, P.H. Wiersema, Effect of hydrodynamic interaction on coagulation rate of hydrophobic colloids, J. Colloid Interface Sci. 36 (1971) 97–109.
[31] V. Runkana, P. Somasundaran, P.C. Kapur, Reaction-limited aggregation in presence of short-range structural forces, AIChE J. 51 (2005) 1233–1245.
[32] F. Zhang, S.W. Chan, J.E. Spanier, E. Apak, Q. Jin, R.D. Robinson, I.P. Herman, Cerium oxide nanoparticles: size-selective formation and structure analysis, Appl. Phys. Lett. 80 (2002) 127–129.
[33] K.M. Buettner, C.I. Rinciog, S.E. Mylon, Aggregation kinetics of cerium oxide nanoparticles in monovalent and divalent electrolytes, Colloids Surf. A: Physicochem. Eng. Aspects 366 (2010) 74–79.
[34] L. Moller, H.L. Karlsson, P. Cronholm, J. Gustafsson, Copper oxide nanoparticles are highly toxic: a comparison between metal oxide nanoparticles and carbon nanotubes, Chem. Res. Toxicol. 21 (2008) 1726–1732.
[35] Q.L. Li, M. Elimelech, Organic fouling and chemical cleaning of nanofiltration membranes: Measurements and mechanisms, Environ. Sci. Technol. 38 (2004) 4683–4693.
[36] X.Y. Liu, M. Wazne, C. Christodoulatos, K.L. Jasinkiewicz, Aggregation and deposition behavior of boron nanoparticles in porous media, J. Colloid Interface Sci. 330 (2009) 90–96.
[37] A.J. Pelley, N. Tufenkji, Effect of particle size and natural organic matter on the migration of nano- and microscale latex particles in saturated porous media, J. Colloid Interface Sci. 321 (2008) 74–83.
[38] M. Elimelech, C.R. Omelia, Effect of electrolyte type on the electrophoretic mobility of polystyrene latex colloids, Colloids Surf. 44 (1990) 165–178.
[39] B. Kirby, Micro- and Nanoscale Fluid Bechanics: Transport in Microfluidic Devices, 1st ed., Cambridge University Press, NY, USA, 2010.
[40] N.B. Saleh, L.D. Pfefferle, M. Elimelech, Influence of biomacromolecules and humic acid on the aggregation kinetics of single-walled carbon nanotubes, Environ. Sci. Technol. 44 (2010) 2412–2418.
[41] E. Tipping, M. Ohnstad, Colloid stability of iron-oxide particles from a freshwater lake, Nature 308 (1984) 266–268.
[42] X.Y. Liu, M. Wazne, T.M. Chou, R. Xiao, S.Y. Xu, Influence of Ca^{2+} and Suwannee River humic acid on aggregation of silicon nanoparticles in aqueous media, Water Res. 45 (2011) 105–112.
[43] T. Phenrat, N. Saleh, K. Sirk, H.J. Kim, R.D. Tilton, G.V. Lowry, Stabilization of aqueous nanoscale zerovalent iron dispersions by anionic polyelectrolytes: adsorbed anionic polyelectrolyte layer properties and their effect on aggregation and sedimentation, J. Nanopart. Res. 10 (2008) 795–814.
[44] H. Ohshima, Electrophoresis of soft particles, Adv. Colloid Interface Sci. 62 (1995) 189–235.
[45] T. Phenrat, J.E. Song, C.M. Cisneros, D.P. Schoenfelder, R.D. Tilton, G.V. Lowry, Estimating attachment of nano- and submicrometer-particles coated with organic macromolecules in porous media: development of an empirical model, Environ. Sci. Technol. 44 (2010) 4531–4538.
[46] A.L. Ahmad, M.F. Chong, S. Bhatia, Population Balance Model (PBM) for flocculation process: simulation and experimental studies of palm oil mill effluent (POME) pretreatment, Chem. Eng. J. (Lausanne) 140 (2008) 86–100.
[47] T. Cosgrove, T.L. Crowley, K. Ryan, J.R.P. Webster, The effects of solvency on the structure of an adsorbed polymer layer and dispersion stability, Colloids Surf. 51 (1990) 255–269.
[48] H. Karimian, A.A. Babaluo, Halos mechanism in stabilizing of colloidal suspensions: nanoparticle weight fraction and pH effects, J. Eur. Ceram. Soc. 27 (2007) 19–25.
[49] J. Klein, G. Rossi, Analysis of the experimental implications of the scaling theory of polymer adsorption, Macromolecules 31 (1998) 1979–1988.
[50] E.M.V. Hoek, G.K. Agarwal, Extended DLVO interactions between spherical particles and rough surfaces, J. Colloid Interface Sci. 298 (2006) 50–58.
[51] A. Revil, P.A. Pezard, P.W.J. Glover, Streaming potential in porous media 1. Theory of the zeta potential, J. Geophys. Res. – Solid Earth 104 (1999) 20021–20031.
[52] Y.Q. Hao, Y.F. Wang, Y.X. Weng, Particle-size-dependent hydrophilicity of TiO_2 nanoparticles characterized by Marcus reorganization energy of interfacial charge recombination, J. Phys. Chem. C 112 (2008) 8995–9000.
[53] M. Berka, J.A. Rice, Relation between aggregation kinetics and the structure of kaolinite aggregates, Langmuir 21 (2005) 1223–1229.
[54] M.Y. Lin, H.M. Lindsay, D.A. Weitz, R.C. Ball, R. Klein, P. Meakin, Universality in colloid aggregation, Nature 339 (1989) 360–362.
[55] M.Y. Lin, H.M. Lindsay, D.A. Weitz, R. Klein, R.C. Ball, P. Meakin, Universal diffusion-limited colloid aggregation, J. Phys.: Condens. Matter 2 (1990) 3093–3113.
[56] P. Sandkuhler, J. Sefcik, M. Lattuada, H. Wu, M. Morbidelli, Modeling structure effects on aggregation kinetics in colloidal dispersions, AIChE J. 49 (2003) 1542–1555.